On the Analytical Error Performance of LoRa-Based LEO Satellite IoT

Quantao Yu*, Deepak Mishra†, Hua Wang*, Dongxuan He*, Jinhong Yuan†, and Michail Matthaiou‡
*School of Information and Electronics, Beijing Institute of Technology, Beijing, China
†School of Electrical Engineering and Telecommunications, University of New South Wales, Sydney, Australia
‡Centre for Wireless Innovation (CWI), Queen's University Belfast, BT3 9DT Belfast, U.K.

GLOBECOM 2025 - 2025 IEEE Global Communications Conference | 979-8-3315-7781-0/25/$31.00 ©2025 IEEE | DOI: 10.1109/GLOBECOM59602.2025.11432131

***Abstract*—Recently, Long-Range (LoRa)-based low Earth orbit (LEO) satellite Internet-of-Things (IoT) has been recognized as a key enabler to provide ubiquitous connectivity for the Internet of remote things. A rigorous error performance analysis of such a new paradigm is quite essential for its practical implementation and evaluation. In this paper, we propose a novel analytical framework for quantitatively characterizing the error performance of LoRa-based LEO satellite IoT systems by leveraging an empirically-verified satellite-to-ground channel model, where both the channel characteristics of near-Earth satellite communications and the waveform properties of LoRa modulation are considered. Moreover, to enable a practical analysis, inter-end device interference is taken into account in the presence of both time and frequency offsets. Based on this, closed-form symbol and bit error rate expressions are derived by approximating the impact of the overall interference distributed within the decision metrics to that of the peak interference. Numerical simulations not only validate our theoretical analysis but also provide further insights into the error performance improvements of LoRa-based LEO satellite IoT systems.**

***Index Terms*—Error performance, Internet of remote things, LoRa, near-Earth satellite communications.**

I. Introduction

With the rapid evolution of the Internet of remote things, LoRa-based LEO satellite IoT has been regarded as a key enabler to provide ubiquitous connectivity in rural and remote areas, and, hence, has attracted widespread attention from both academia and industry [1]. Over the past few years, various methods have been proposed [2] to improve the link-level and/or system-level performance of LoRa-based LEO satellite IoT systems, either from the physical (PHY) layer perspective, including the chirp spread spectrum (CSS)-based waveform design [3] and signal detection [4], or from the medium access control (MAC) layer perspective, like the random access (RA)-based protocol design [5]. Nonetheless, few studies have focused on a rigorous error performance analysis of the underlying LoRa-based LEO satellite IoT system [6], which, however, is quite important for the practical implementation and evaluation of such a new paradigm.

This work was supported in part by the National Key Research and Development Program of China under Grant 2024YFE0200404; in part by the National Key Research and Development Program of China under Grant 2020YFB1807900; in part by the China Scholarship Council (CSC); and in part by the U.K. Engineering and Physical Sciences Research Council (grant No. EP/X04047X/1). This work was partially funded by the Australian Research Council (ARC) Discovery Early Career Researcher Award - DE230101391. The work of M. Matthaiou has received funding from the European Research Council (ERC) under the European Union's Horizon 2020 research and innovation programme (grant agreement No. 101001331).

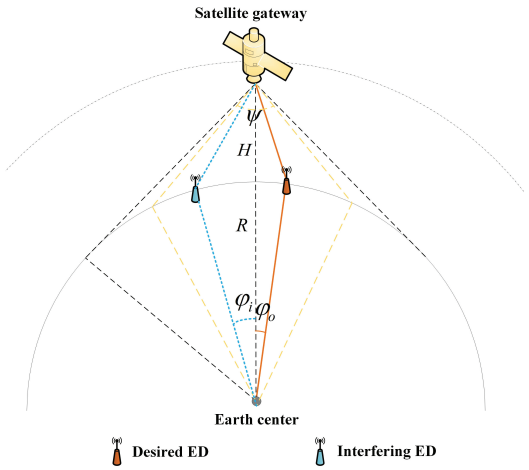

Fig. 1. An illustration of the network model of the considered LoRa-based LEO satellite IoT system.

A. State-of-the-Art

To characterize the error performance of LoRa-based systems under different conditions, researchers have conducted various studies on the impact of noise, interference, and channel fading. For example, Elshabrawy and Robert [7] derived closed-form approximations for the bit error rate (BER) performance of LoRa modulation over both additive white Gaussian noise (AWGN) and Rayleigh fading channels. Furthermore, the authors in [8] derived analytical expressions for the symbol error rate (SER) and BER of LoRa modulation in the presence of AWGN and the same spreading factor (co-SF) interference. In addition, approximate BER expressions of LoRa modulation under the impact of carrier frequency offset (CFO) were derived in [9]. More recently, closed-form BER expressions of a multi-reconfigurable intelligent surface (RIS)-assisted LoRa system were derived in [10] under the impact of outdated and imperfect channel state information (CSI). However, none of these works considered the channel characteristics of near-Earth satellite communications, which significantly limit their applicability for LEO satellite IoT scenarios. To our best knowledge, a rigorous error performance analysis of LoRa-based LEO satellite IoT systems has not been well investigated in the existing literature.

B. Motivation and Contributions

To fill this gap, we present a novel analytical framework in this paper to characterize the error performance of LoRa-based

LEO satellite IoT systems, and thereby facilitate their practical implementation and evaluation. The underlying investigated system is crucial for supporting various critical applications such as environmental monitoring, precision agriculture, and disaster prevention by delivering ubiquitous connectivity. The main contributions of this paper are summarized as follows:

1) A novel analytical framework for characterizing the error performance of LoRa-based LEO satellite IoT systems is developed by leveraging an empirically-verified satellite-to-ground channel model. Both the channel characteristics of near-Earth satellite communications and the waveform properties of LoRa modulation are considered.
2) To enable a practical analysis, inter-end device (inter-ED) interference is modeled in the presence of both time and frequency offsets. Based on this, closed-form symbol and bit error rate expressions are derived by approximating the impact of the overall interference distributed within the decision metrics to that of the peak interference.
3) Numerical simulations are conducted, which not only validate the accuracy of our theoretical analysis but also provide further insights into the error performance improvements of LoRa-based LEO satellite IoT systems.

II. Preliminaries

LoRa adopts CSS modulation with the following two important parameters:

- B is the bandwidth of the LoRa modulation signal.
- k is the SF of LoRa modulation ranging from 7 to 12.

Under Nyquist sampling, each chirp can be defined by $M = 2^k$ samples in the complex base-band equivalent form, and the basic upchirp can be expressed as [11]

$$u[n] = \exp\left\{j\frac{\pi n^2}{M}\right\}, \tag{1}$$

where $n = 0, 1, ..., M-1$ is the sample index.

In LoRa modulation, M orthogonal upchirps are used to represent the modulation symbols. Without loss of generality, every k information bits $b_0, b_1, ..., b_{k-1}$ are mapped to a data symbol as $m = \sum_{i=0}^{k-1} b_i 2^i \in \mathcal{L} = \{0, 1, ..., M-1\}$, and thereby the modulation signal is given by [11]

$$s_m[n] = u[n]\exp\left\{j\frac{2\pi mn}{M}\right\} = \exp\left\{j\pi\frac{n^2+2mn}{M}\right\}. \tag{2}$$

After passing through an AWGN channel, the received signal can be expressed as

$$r_m[n] = s_m[n] + w[n], \tag{3}$$

where $w[n]$ is the complex circularly symmetric additive white Gaussian noise with zero mean and variance σ_q^2. Note that $\sigma_q^2 = -174 + N_F + 10\log_{10} B$, with N_F representing the receiver's noise figure.

Then, the signal detection for each modulation symbol can be divided into three steps, i.e., dechirp, discrete Fourier transform (DFT), and frequency domain (FD) peak index decision. Specifically, the received signal is first multiplied by the complex conjugate of the basic upchirp, i.e., dechirp operation, and then an M-point DFT operation is performed on the dechirped signal, yielding

$$\begin{aligned} R_m[l] &= \sum_{n=0}^{M-1} r_m[n]u^*[n]\exp\left\{-j\frac{2\pi ln}{M}\right\} \\ &= \begin{cases} M + W[m], & l = m, \\ W[l], & l \neq m, \end{cases} \end{aligned} \tag{4}$$

where $W[l] = \sum_{n=0}^{M-1} w[n]u^*[n]\exp\left\{-j\frac{2\pi ln}{M}\right\} \sim \mathcal{CN}(0, \sigma^2)$ with $\sigma^2 = M\sigma_q^2$.

Finally, the data symbol can be estimated as [11]

$$\hat{m} = \arg\max_{l\in\mathcal{L}} |R_m[l]|, \tag{5}$$

for non-coherent detection, with $|\cdot|$ here representing the absolute value operation.

III. System Model

A. Network Model

As shown in Fig. 1, we consider a single LEO satellite that directly communicates with the desired LoRa ED within its coverage region.[1] Without loss of generality, we denote H as the orbit altitude while the coverage region is determined by the satellite effective beamwidth, which corresponds to the maximum satellite-centric angle ψ. Moreover, there are other interfering LoRa EDs distributed within the satellite footprint which may cause inter-ED interference to the desired LoRa ED. In general, for our considered LoRa-based LEO satellite IoT system, inter-ED interference consists of co-SF and inter-SF interference. Given the waveform properties of LoRa modulation, inter-SF interference can be assumed to be negligible since different SFs are quasi-orthogonal [13]. Furthermore, the impact of accumulative interference caused by multiple co-SF EDs can be effectively approximated by that of the strongest one [13]. Accordingly, we can only consider the impact of one co-SF interfering ED for interference characterization. Also, we use the contact angle φ to denote the relative location between an ED and satellite, i.e., the Earth-centered zenith angle. According to the basic sine theorem, the maximum contact angle φ_m can be derived as [14]

$$\varphi_m(\psi) = \begin{cases} \sin^{-1}\left(\frac{R+H}{R}\sin\left(\frac{\psi}{2}\right)\right) - \frac{\psi}{2}, & \text{if } \psi < \psi_0, \\ \cos^{-1}\left(\frac{R}{R+H}\right), & \text{if } \psi \geq \psi_0, \end{cases} \tag{6}$$

where R is the radius of Earth and $\psi_0 = 2\sin^{-1}\left(\frac{R}{R+H}\right)$ denotes the effective beamwidth that corresponds to just covering the horizon. Moreover, given the contact angle φ, the distance between an ED and satellite can be obtained using the basic cosine theorem as [14]

$$d(\varphi) = \sqrt{(R+H)^2 + R^2 - 2R(R+H)\cos\varphi}. \tag{7}$$

[1]Note that the subsequent performance analysis is also applicable to multiple LEO satellite systems. Specifically, for the network model of LEO satellite constellations, each LoRa ED can be assumed to be associated with its nearest satellite (i.e., desired ED), while the other LoRa EDs within the coverage region of the serving satellite are interfering EDs [12].

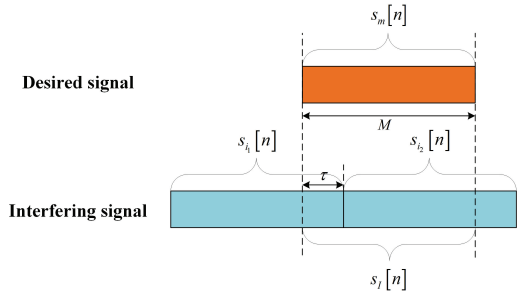

Fig. 2. An illustration of the time domain signal collision model.

B. Channel Model

For the satellite-to-ground channel model within our considered LoRa-based LEO satellite IoT system, we follow a newly developed empirically-verified model adopted in [14], [15], which leverages the recent developments in satellite-to-ground path-loss modeling and line-of-sight (LoS) probability formulation. In particular, both the free-space path loss (FSPL) and the excess path-loss (EPL) are taken into account, which extends the applicability of our channel model in practical scenarios. Specifically, the FSPL is given by

$$L(\varphi) = \left(\frac{c}{4\pi f_c d(\varphi)}\right)^2, \tag{8}$$

where c refers to the speed of light and f_c is the carrier frequency. Moreover, let us denote η as the EPL which follows a mixed Gaussian distribution [15]. Note that given the contact angle φ, the variations of the EPL are considered to be negligible when compared to its mean value. Accordingly, we use the average EPL $\bar{\eta}(\varphi)$ for the sake of simplicity, which can be expressed as [15]

$$\begin{aligned}\bar{\eta}(\varphi) = {} & p_{LoS}(\varphi)\exp\left(\frac{\zeta^2\sigma_{LoS}^2}{2} - \delta\mu_{LoS}\right) \\ & + \left(1 - p_{LoS}(\varphi)\right)\exp\left(\frac{\zeta^2\sigma_{NLoS}^2}{2} - \delta\mu_{NLoS}\right),\end{aligned} \tag{9}$$

where $\zeta \triangleq \frac{\ln(10)}{10}$, $p_{LoS}(\varphi) = \exp\left(-\frac{\beta\sin\varphi}{\cos\varphi - \alpha}\right)$ is the probability of LoS transmission, $\alpha = \frac{R}{R+H}$, while the parameters $\mu_{LoS}, \sigma_{LoS}, \mu_{NLoS}, \sigma_{NLoS}, \beta$ depend on the specific propagation environment [15].

C. Signal Model

As depicted in Fig. 1, φ_o and φ_i are the contact angles of the desired and interfering ED. Moreover, let P_o, G_o and P_i, G_i denote the transmit power and antenna gain of the desired and interfering ED, respectively. Then, the received signal at the satellite gateway can be expressed as

$$\begin{aligned}r_m[n] = {} & \underbrace{\sqrt{P_o G_o G_s L(\varphi_o)\bar{\eta}(\varphi_o)}s_m[n]}_{\text{desired signal}} + \underbrace{w[n]}_{\text{noise}} \\ & + \underbrace{\sqrt{P_i G_i G_s L(\varphi_i)\bar{\eta}(\varphi_i)}s_I[n]\exp\left\{j2\pi n\frac{\epsilon}{M}\right\}}_{\text{interfering signal}},\end{aligned} \tag{10}$$

where G_s represents the satellite antenna gain, $s_m[n]$ and $s_I[n]$ are the transmitted LoRa signals of the desired and interfering ED, respectively, and ϵ denotes the normalized relative frequency offset (FO) between them. Notably, the normalization is carried out with respect to $\Delta f = \frac{B}{M} = \frac{1}{T}$, where T is the symbol duration. Herein, we point out that both laboratory and flight testing have verified the strong immunity of LoRa-based LEO satellite communications to the Doppler effect [16], [17]. Namely, by availing of the effective synchronization algorithms employed in LoRa PHY layer, the Doppler effect can be properly handled in LoRa-based DtS-IoT communications. Therefore, the onboard gateway is assumed to be synchronized with the desired signal, which is a common assumption in many research works concerning interference-limited LoRa systems [8], [13]. As such, the uncoordinated transmission will inevitably lead to relative time and frequency offsets between the desired and interfering LoRa signals. Specifically, the relative FO can be decomposed into integer and fractional parts. As pointed out in [9], the integer FO simply leads to a cyclic shift of the peak index in the DFT output without energy spread. Consequently, we can only consider the impact of fractional FO, i.e., $\epsilon \in [0, 0.5]$, which causes energy spread due to the lack of DFT resolution. So, the time domain signal collision model is illustrated in Fig. 2, where the interfering signal is composed of two different LoRa symbols during each period of the desired signal due to the asynchronous transmission. Without loss of generality, we assume that the relative time offset (TO) τ is an integer randomly distributed between 0 and $M-1$, and thus we have

$$s_I[n] = \begin{cases} s_{i_1}[n], & 0 \le n < \tau, \\ s_{i_2}[n], & \tau \le n < M-1, \end{cases} \tag{11}$$

where $i_1, i_2 \in \mathcal{L}$ are the data symbols of interfering signal.

IV. Performance Analysis

Here, the theoretical error performance of the LoRa-based LEO satellite IoT system is investigated. To this end, the decision metrics are first derived within the underlying system model.

A. Decision Metrics

With $J_o = \sqrt{P_o G_o G_s L(\varphi_o)\bar{\eta}(\varphi_o)}M$ and $J_i = \sqrt{P_i G_i G_s L(\varphi_i)\bar{\eta}(\varphi_i)}$, the DFT output of the dechirped signal for a given m as obtained using (4), (10), (11) is

$$\begin{aligned}R_m[l] &= \sum_{n=0}^{M-1} r_m[n]u^*[n]\exp\left\{-j\frac{2\pi ln}{M}\right\} \\ &= J_o\delta[l-m] + J_i\mathcal{I}[l] + W[l],\end{aligned} \tag{12}$$

where

$$\begin{aligned}\mathcal{I}[l] &= \sum_{n=0}^{\tau-1} e^{j\frac{2\pi n(i_1-l+\epsilon)}{M}} + \sum_{n=\tau}^{M-1} e^{j\frac{2\pi n(i_2-l+\epsilon)}{M}} \\ &\overset{(a)}{=} \frac{\sin\left[\pi(i_1-l+\epsilon)\tau/M\right]}{\sin\left[\pi(i_1-l+\epsilon)/M\right]}\Phi_I \\ &\quad + \frac{\sin\left[\pi(i_2-l+\epsilon)(M-\tau)/M\right]}{\sin\left[\pi(i_2-l+\epsilon)/M\right]}\Phi_{II},\end{aligned} \tag{13}$$

is the interfering term in the DFT output, step (a) follows from the geometric series, $\delta[\cdot]$ is the Kronecker delta function, $W[l] \sim \mathcal{CN}(0, \sigma^2)$, $\Phi_I = \exp\{j\pi(i_1 - l + \epsilon)(\tau - 1)/M\}$, and $\Phi_{II} = \exp\{j\pi(i_2 - l + \epsilon)(M + \tau - 1)/M\}$.

Therefore, the recovered data symbol can be determined as

$$\hat{m} = \arg\max_{l \in \mathcal{L}} \left| J_o \delta[l - m] + J_i \mathcal{I}[l] + W[l] \right|, \tag{14}$$

for non-coherent detection.

B. Analytical Error Rate Expressions

According to (12), the decision metric $|R_m[l]|$ follows a Rician distribution with the Rician factor $\kappa_m = \frac{J_o^2 + J_i^2 |\mathcal{I}[m]|^2}{\sigma^2}$ for $l = m$ and $\kappa_l = \frac{J_i^2 |\mathcal{I}[l]|^2}{\sigma^2}$ for $l \neq m$. For $l = m$, $|R_m[l]|$ can be approximated by a Gaussian random variable with mean $J_o + J_i|\mathcal{I}[m]|$ and variance $\frac{\sigma^2}{2}$. For $l \neq m$, the frequency bins of the DFT output can be divided into two sets, namely, interference-driven set $S_I = \{\kappa_l \geq \Xi, l \neq m\}$ and noise-driven set $S_N = \{\kappa_l < \Xi, l \neq m\}$, based on the value of κ_l [9]. More specifically, for $l \in S_I$, $|R_m[l]|$ can be approximated by a Gaussian random variable with mean $J_i|\mathcal{I}[l]|$ and variance $\frac{\sigma^2}{2}$, while for $l \in S_N$, $|R_m[l]|$ can be approximated by a Rayleigh random variable. Let us denote $\rho = \max_{l \in S_N} |R_m[l]|$ and using a moment matching method, ρ is approximated by a Gaussian random variable with mean [7]

$$\mu_\rho = \sigma \left(H_{|S_N|}^2 - \frac{H_{|S_N|}^{(2)}}{2} \right)^{\frac{1}{4}}, \tag{15}$$

and variance

$$\sigma_\rho^2 = \sigma^2 \left(H_{|S_N|} - \sqrt{H_{|S_N|}^2 - \frac{H_{|S_N|}^{(2)}}{2}} \right), \tag{16}$$

respectively, where $H_{|S_N|} = \sum_{i=1}^{|S_N|} \frac{1}{i}$ is the N-th harmonic number and $H_{|S_N|}^{(2)} = \sum_{i=1}^{|S_N|} \frac{1}{i^2}$, with $|\cdot|$ here denoting the cardinality of a set. In addition, we approximate the impact of the overall interference distributed within the decision metrics by that of the peak interference appearing at a certain frequency bin to further simplify our analysis. Specifically, we assume that the interfering term $\mathcal{I}[l]$ exhibits a peak magnitude at a certain frequency bin $\widetilde{m} \neq m$ for each realization of i_1, i_2, m, and τ, while its magnitudes over the remaining frequency bins can be negligible. The accuracy of this approximation will be shown in Section V through numerical simulations. Moreover, regarding the peak magnitude of the interfering term, we have the following proposition.

Proposition 1. *The upper bound on the magnitude of the interfering term $\mathcal{I}[l]$ can be obtained as*

$$|\mathcal{I}[l]| \leq \Lambda_{\chi,\tau} = \left| \frac{\sin(\pi\chi\tau/M)}{\sin(\pi\chi/M)} \right| + M - \tau, \tag{17}$$

where χ is uniformly distributed in $\mathcal{L}$, while τ is an integer uniformly distributed within $\left[0, \frac{M}{2}\right)$.

Proof: See Appendix. ∎

Hence, the DFT output of (12) becomes

$$R_{m,\widetilde{m}}[l] = \begin{cases} J_o + W[m], & l = m, \\ J_i \Lambda_{\chi,\tau} + W[\widetilde{m}], & l = \widetilde{m}, \\ W[l], & l \neq m, \widetilde{m}. \end{cases} \tag{18}$$

Therefore, the approximate SER can be divided into noise-driven SER, $\widetilde{P}_s^N$, and interference-driven SER, $\widetilde{P}_s^I$, respectively. On one hand, the noise-driven SER, $\widetilde{P}_s^N$, can be obtained according to (15), (16) and (18) as

$$\begin{aligned} \widetilde{P}_s^N &= \mathbb{P}\left\{ \max_{l \neq m, \widetilde{m}} |W[l]| > |J_o + W[m]| \right\} \\ &\overset{(a)}{\approx} Q\left(\frac{J_o - \sigma\left(H_{M-2}^2 - \frac{\pi^2}{12}\right)^{\frac{1}{4}}}{\sqrt{\frac{\sigma^2}{2} + \sigma^2\left(H_{M-2} - \sqrt{H_{M-2}^2 - \frac{\pi^2}{12}}\right)}} \right). \end{aligned} \tag{19}$$

where $Q(\cdot)$ is the Gaussian Q-function, step (a) follows from $|S_N| = M - 2 \gg 1$ whereas $H_{|S_N|}^{(2)}$ will converge to $\frac{\pi^2}{6}$ for a sufficiently large $|S_N|$. On the other hand, the conditional interference-driven SER can be obtained according to (18) as

$$\begin{aligned} \widetilde{P}_s^{I|\chi,\tau} &= \mathbb{P}\left\{ \left| J_i \Lambda_{\chi,\tau} + W[\widetilde{m}] \right| > \left| J_o + W[m] \right| \right\} \\ &\approx Q\left(\frac{J_o - J_i \Lambda_{\chi,\tau}}{\sigma} \right). \end{aligned} \tag{20}$$

As such, the approximate interference-driven SER, $\widetilde{P}_s^I$, can be computed as

$$\widetilde{P}_s^I \approx \frac{2}{M^2} \sum_{\chi=0}^{M-1} \sum_{\tau=0}^{\frac{M}{2}-1} Q\left(\frac{J_o - J_i \Lambda_{\chi,\tau}}{\sigma} \right). \tag{21}$$

Since the noise-driven SER, $\widetilde{P}_s^N$, and interference-driven SER, $\widetilde{P}_s^I$, are independent, the closed-form BER expression can be obtained by combining (19) and (21) as

$$\widetilde{P}_b = \frac{M}{2(M-1)} \left[1 - \left(1 - \widetilde{P}_s^N\right)\left(1 - \widetilde{P}_s^I\right) \right]. \tag{22}$$

Remark 1: When the interfering ED is outside the satellite footprint, no interference-driven error occurs, which represents an ideal interference-free scenario, and thus the approximate BER becomes[2]

$$\widetilde{P}_b^* \approx \zeta Q\left(\frac{J_o - \sigma\left(H_{M-1}^2 - \frac{\pi^2}{12}\right)^{\frac{1}{4}}}{\sqrt{\frac{\sigma^2}{2} + \sigma^2\left(H_{M-1} - \sqrt{H_{M-1}^2 - \frac{\pi^2}{12}}\right)}} \right), \tag{23}$$

which will go to zero with the increase of P_o since $J_o = \sqrt{P_o G_o G_s L(\varphi_o)\,\overline{\eta}(\varphi_o)} M$.

[2]Note that $|S_N| = M - 1$ in the absence of interference.

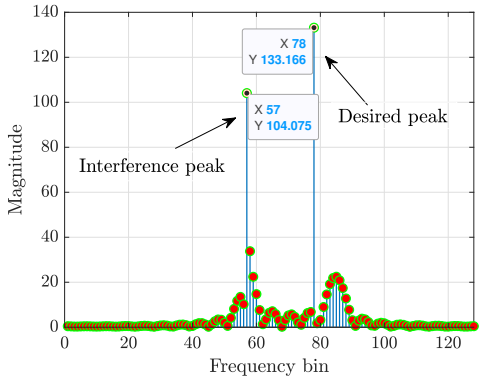

(a) $N_i = 1$

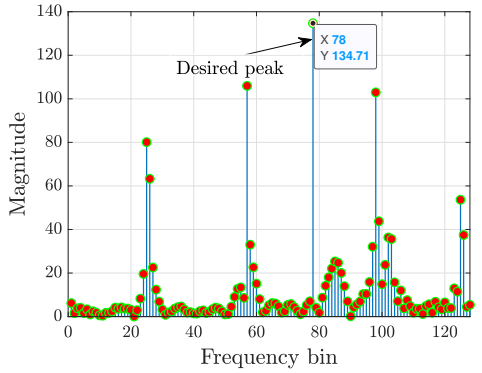

(b) $N_i = 4$

Fig. 3. DFT output for $P_o = 14$ dBm, $\varphi_o = 0°$, $SF = 7$, and $m = 78$ with the number of interfering EDs: (a) $N_i = 1$ and (b) $N_i = 4$.

V. Numerical Simulations and Discussion

In this section, we validate our theoretical performance analysis through Monte-Carlo simulations under practical system parameters. The simulation setup is illustrated as follows. Unless otherwise specified, we set $R = 6371$ km, $H = 500$ km, $\psi = 50°$, $f_c = 868$ MHz, $B = 125$ kHz, $\epsilon = 0.5$, $P_i = 14$ dBm, $N_F = 6$ dB, $G_s = 10$ dBi, $G_o = G_i = 2.15$ dBi, $\varphi_i = 0°$, $\beta = 2.3$, $\mu_{LoS} = 0$ dB, $\sigma_{LoS} = 2.8$ dB, $\mu_{NLoS} = 12$ dB, and $\sigma_{NLoS} = 9$ dB, where the majority of these parameters are in accordance with [11], [14], [15].

First, Figs. 3(a) and 3(b) show that the impact of the overall interference distributed within the decision metrics can be approximated by that of the peak interference appearing at a certain frequency bin, where N_i denotes the number of interfering EDs. For $N_i = 1$ (i.e., relatively sparse deployment), a specific example for $\tau = 105$, $i_1 = 34$, and $i_2 = 62$ is shown in Fig. 3(a). It can be observed that the overall interference distributed within the decision metrics, i.e., $|\mathcal{I}[l]|$, exhibits a peak magnitude at a certain frequency bin $\widetilde{m} \neq m$ while its magnitudes over the remaining frequency bins can be approximately negligible. Furthermore, for $N_i = 4$ (i.e., relatively dense deployment), more interference peaks appear in the DFT output as illustrated in Fig. 3(b), while the error margin of the approximation can be amplified.

Fig. 4 demonstrates the BER performance of our considered

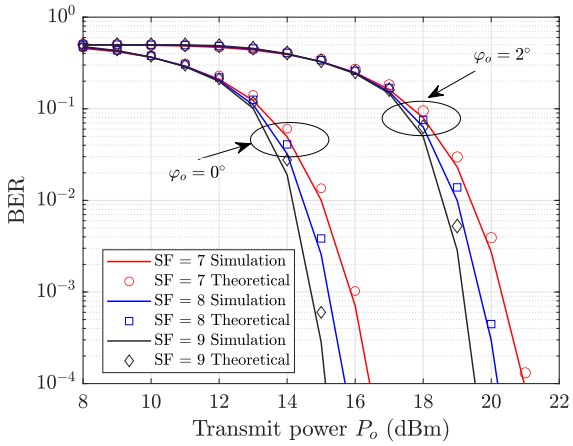

Fig. 4. BER performance of LoRa-based LEO satellite IoT system versus P_o for $B = 125$ kHz.

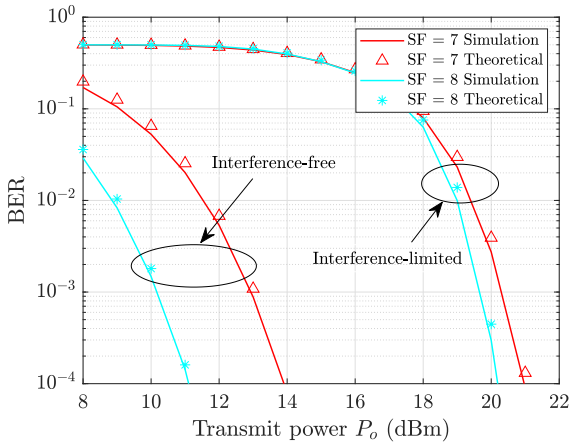

Fig. 5. BER performance versus P_o with and without interference for $H = 500$ km, $B = 125$ kHz, and $\varphi_o = 2°$.

LoRa-based LEO satellite IoT system versus P_o for $B = 125$ kHz. It can be observed that the numerical results match well with the analytical results, which substantiates our theoretical analysis. Furthermore, it can be seen that the BER performance of our considered LoRa-based LEO satellite IoT system improves with the increase of the SF due to the larger spreading gain of CSS modulation. It can be further noticed that the contact angle of the desired ED, i.e., ED's location, has a remarkable impact on the system error performance because as φ_o increases, the desired signal quality decreases due to the amplified satellite-to-ground path-loss, while the impact of interfering signal becomes more dominant, thus leading to an error performance degradation.

Fig. 5 compares the BER performance of our considered LoRa-based LEO satellite IoT system with and without interference for $H = 500$ km, $B = 125$ kHz, and $\varphi_o = 2°$. The simulation results in interference-free scenarios also agree well with the theoretical results, which verifies our analysis once again. Furthermore, it can be observed that the underlying system is very sensitive to the inter-ED interference, where a severe performance degradation appears in interference-limited scenarios when compared to

interference-free scenarios. Specifically, the performance loss is around 7 dB and 9 dB for $SF = 7$ and $SF = 8$ at the BER level of 10^{-4}, respectively, which leads to an increased energy consumption for resource-limited IoT EDs. Moreover, a devastating impact on the system error performance will appear when the effect of inter-ED interference becomes more dominant. Therefore, it is of great significance to meticulously investigate the interference suppression techniques in LoRa-based LEO satellite IoT systems, with the deep learning (DL)-based interference mitigation method emerging as a potential solution to further improve the error performance [18].

VI. Conclusion

In this paper, a novel analytical framework for characterizing the error performance of LoRa-based LEO satellite IoT systems was developed. Closed-form analytical symbol and bit error rate expressions were derived, which can provide useful guidelines for the practical implementation and evaluation of such a new paradigm. Numerical simulations were conducted to verify the accuracy of our theoretical analysis, while the impacts of some key system parameters on the error performance were thoroughly investigated. Overall, we believe that our work will set a solid foundation for further investigations of LoRa-based LEO satellite IoT systems, which represent a promising solution for the Internet of remote things.

Appendix

An upper bound on $|\mathcal{I}[l]|$ can be obtained by applying the absolute value inequality to (13) as

$$\begin{aligned}|\mathcal{I}[l]| \leq &\left|\frac{\sin\left[\pi\left(i_1-l+\epsilon\right)\tau/M\right]}{\sin\left[\pi\left(i_1-l+\epsilon\right)/M\right]}\right| \\ &+\left|\frac{\sin\left[\pi\left(i_2-l+\epsilon\right)\left(M-\tau\right)/M\right]}{\sin\left[\pi\left(i_2-l+\epsilon\right)/M\right]}\right|.\end{aligned} \tag{24}$$

As pointed out in [9], the fractional FO ϵ leads to energy spread in the DFT output, where the energy of a certain frequency bin diffuses into other frequency bins due to the lack of DFT resolution, while the whole energy remains unchanged. Therefore, we have

$$\max_{l\in\mathcal{L}}\left\{|\mathcal{I}[l]|\right\} \leq \max_{l\in\mathcal{L}}\left\{\Lambda[l]\right\}, \tag{25}$$

with

$$\Lambda[l]=\underbrace{\left|\frac{\sin\left[\pi\left(i_1-l\right)\tau/M\right]}{\sin\left[\pi\left(i_1-l\right)/M\right]}\right|}_{\Delta_I}+\underbrace{\left|\frac{\sin\left[\pi\left(i_2-l\right)\left(M-\tau\right)/M\right]}{\sin\left[\pi\left(i_2-l\right)/M\right]}\right|}_{\Delta_{II}} \tag{26}$$

where Δ_I and Δ_{II} have maximum values τ and $M-\tau$ at $l = i_1$ and $l = i_2$, respectively. Moreover, we assume that the interfering term exhibits a peak magnitude at a certain frequency bin $\widetilde{m} \neq m$ for each realization of i_1, i_2, m, and τ, whose magnitudes over the remaining frequency bins can be considered negligible. Mathematically speaking, we have

$$\Lambda[l] \approx \begin{cases} \Lambda_{\widetilde{m}}, & l=\widetilde{m}, \\ 0, & l\neq\widetilde{m}. \end{cases} \tag{27}$$

Without loss of generality, we assume $0 \leq \tau < \frac{M}{2}$ and hence, $\Lambda_{\widetilde{m}}$ can be approximated as

$$\Lambda_{\widetilde{m}} \approx \Lambda[i_2] = \left|\frac{\sin\left[\pi\left(i_1-i_2\right)\tau/M\right]}{\sin\left[\pi\left(i_1-i_2\right)/M\right]}\right| + M - \tau. \tag{28}$$

Let $\chi = |i_1 - i_2|$ such that (28) can be further simplified as

$$\Lambda_{\widetilde{m}} = \Lambda_{\chi,\tau} = \left|\frac{\sin\left(\pi\chi\tau/M\right)}{\sin\left(\pi\chi/M\right)}\right| + M - \tau. \tag{29}$$

The proof is completed.

References

[1] M. Asad Ullah, K. Mikhaylov, and H. Alves, "Massive machine-type communication and satellite integration for remote areas," *IEEE Wireless Commun.*, vol. 28, no. 4, pp. 74-80, Aug. 2021.

[2] Y. Xiao, D. Mishra, J. Yuan and Y. Luo, "Proportionally Fair Robust Beamforming for Multicast Multibeam Satellite Systems," *IEEE Commun. Lett.*, vol. 26, no. 1, pp. 128-132, Jan. 2022.

[3] A. Maleki, H. H. Nguyen, E. Bedeer, and R. Barton, "A tutorial on chirp spread spectrum modulation for LoRaWAN: Basics and key advances," *IEEE Open J. Commun. Soc.*, vol. 5, pp. 4578-4612, Jul. 2024.

[4] K. Dakic, B. Al Homssi, S. Walia, and A. Al-Hourani, "Spiking neural networks for detecting satellite Internet of things signals," *IEEE Trans. Aerosp. Electron. Syst.*, vol. 60, no. 1, pp. 1224-1238, Feb. 2024.

[5] S. Herrería-Alonso, M. Rodríguez-Pérez, R. F. Rodríguez-Rubio, and F. Pérez-Fontán, "Improving uplink scalability of LoRa-based direct-to-satellite IoT networks," *IEEE Internet Things J.*, vol. 11, no. 7, pp. 12526-12535, Apr. 2024.

[6] Q. Yu, D. Mishra, H. Wang, D. He, J. Yuan and M. Matthaiou, "Toward LoRa-Based LEO Satellite IoT: A Stochastic Geometry Perspective," *IEEE Internet Things J.*, vol. 12, no. 15, pp. 30725-30738, Aug. 2025.

[7] T. Elshabrawy and J. Robert, "Closed-form approximation of LoRa modulation BER performance," *IEEE Commun. Lett.*, vol. 22, no. 9, pp. 1778-1781, Sept. 2018.

[8] O. Afisiadis, M. Cotting, A. Burg, and A. Balatsoukas-Stimming, "On the error rate of the LoRa modulation with interference," *IEEE Trans. Wireless Commun.*, vol. 19, no. 2, pp. 1292-1304, Feb. 2020.

[9] P. Huang, J. Liu, and B. Ma, "Approximate BER performance of LoRa communication under carrier frequency offset," *IEEE Internet Things J.*, vol. 11, no. 15, pp. 26001-26004, Aug. 2024.

[10] Z. Liang, G. Cai, J. He, G. Kaddoum, and C. Huang, "Performance analysis of multi-RIS-aided LoRa systems with outdated and imperfect CSI," *IEEE Trans. Commun.*, vol. 73, no. 7, pp. 4647-4661, Jul. 2025.

[11] Q. Yu, D. He, Z. Lu, and H. Wang, "SSK-based PSK-LoRa modulation for IoT communications," *IEEE Open J. Commun. Soc.*, vol. 4, pp. 1487-1498, Jul. 2023.

[12] Q. Yu, D. Mishra, H. Wang, D. He, J. Yuan, and M. Matthaiou, "System-Level performance analysis of LoRa-based LEO satellite constellations for IoT communications," *IEEE Wireless Commun. Lett.*, early access.

[13] Z. Liang, G. Cai, J. He, G. Kaddoum, C. Huang, and M. Debbah, "RIS-enabled anti-interference in LoRa systems," *IEEE Trans. Commun.*, vol. 72, no. 10, pp. 6599-6616, Oct. 2024.

[14] B. A. Homssi and A. Al-Hourani, "Modeling uplink coverage performance in hybrid satellite-terrestrial networks," *IEEE Commun. Lett.*, vol. 25, no. 10, pp. 3239-3243, Oct. 2021.

[15] A. Al-Hourani, "An analytic approach for modeling the coverage performance of dense satellite networks," *IEEE Wireless Commun. Lett.*, vol. 10, no. 4, pp. 897-901, Apr. 2021.

[16] A. M. Zadorozhny *et al.*, "First flight-testing of LoRa modulation in satellite radio communications in low-Earth orbit," *IEEE Access*, vol. 10, pp. 100006-100023, Sep. 2022.

[17] Q. Yu, D. Mishra, H. Wang, D. He, J. Yuan, and M. Matthaiou, "Closed-form access probability analysis for LoRa-based LEO satellite IoT," in *Proc. IEEE ICC*, Jun. 2025.

[18] A. A. Tesfay, S. Kharbech, E. P. Simon, and L. Clavier, "Signal denoising and detection for uplink in LoRa networks based on Bayesian-optimized deep neural networks," *IEEE Commun. Lett.*, vol. 27, no. 1, pp. 214-218, Jan. 2023.